Int. J. Electrochem. Sci., 13 **(2018)** 6473 – 6483, doi: 10.20964/2018.07.60

International Journal of
ELECTROCHEMICAL
SCIENCE
www.electrochemsci.org

Electrochemical Corrosion Behavior of Chromium-Free Composite Passivation Film on Galvanized Steel

Liu Zhaohua[1], *Liu Cheng*[2], *Xu Zhengfeng*[1], *Ju Rong*[2], *Xiaohua Yu*[2*], *Zhang Yannan*[2]

[1] Pan Gang Group Research Institute Co., Ltd., State Key Laboratory of Vanadium and Titanium Resources Comprehensive Utilization, Panzhihua 617000, China
[2] National Engineering Research Center of Solid Waste Resources, Kunming University of Science and Technology, Kunming 650093, China.
Liu Zhaohua and Liu Cheng have contributed equally to this paper.
[*]E-mail: xiaohua_y@163.com

Received: 11 February 2018 / *Accepted:* 11 May 2018 / *Published:* 5 June 2018

An eco-friendly and economical chromium-free composite passivation solution was prepared from ammonium molybdate, nanosilica sol, tannic acid, and silane coupling agents KH151 and KH792. This solution was coated onto galvanized steel and the micro-morphology, chemical composition, as well as corrosion resistance of the resulting film were analyzed via various methods. As a novel chromium-free composite passivation film, this coating combined the benefits of molybdate passivation and organosilane passivation. That is, the corrosion electrochemical reaction was inhibited, film exhibited high resistance, reaction speed decreased, and corrosion resistance increased. In addition, Mo inhibited the generation and development of micro-cracks, resulting in improved surface quality. The corrosion resistance of this passivation film was significantly higher than that of the silane passivation film. Furthermore, the optimal corrosion resistance of the galvanized steel was realized at a coating amount of 1252 mg/m^2. This work can serve as a reference for developing passivation technology for galvanized steel.

Keywords: galvanized steel sheet, chromium-free composite passivation film, electrochemical, corrosion resistance

1. INTRODUCTION

Traditional hexavalent chromium passivation technology is highly toxic and harmful to the environment and has therefore been banned worldwide [1]. Eco-friendly chrome-free passivation technology represents an attractive alternative for the galvanizing industry.

The current passivation process consists mainly of trivalent chromium passivation and chrome-free passivation. This chrome-free passivation process may be classified into three categories: molybdate passivation, rare earth salt passivation, and organosilane passivation. Unfortunately, a single chromium-free passivation process yielding an effect equivalent to that of hexavalent chromium passivation remains elusive [2,3]. The effect of trivalent chromium passivation is similar to that of hexavalent chromium, and its toxicity is only 1% that of hexavalent chromium. However, trivalent chromium would be oxidized to hexavalent chromium and, hence, the problem of chromium pollution remains unresolved [4,5]. Molybdate has low toxicity and is therefore considered an effective substitute for chromate, but the corrosion resistance of a single molybdate passivation film is inadequate [6–8]. Rare-earth salts exhibit better corrosion resistance and are safer than the molybdate, but the slow deposition of rare-earth ions renders the passivation process time consuming and costly [9,10]. In contrast, organosilane is low-cost, non-toxic, easily synthesized, and convenient for subsequent treatment. Therefore, in recent years, organosilane passivation has become an ideal candidate for replacing chromate passivation [11–13], although the combination and the tightness of the silane film are poor, leading to inadequate corrosion resistance [14–17].

The purpose of this work is to solve the problem of environmental pollution caused by the hexavalent chromium passivation process. A new and environmentally friendly chromium-free composite passivating solution consisting of several components (including ammonium molybdate, nano silica sol, and tannic acid) is prepared. The microstructure and chemical composition of the chromium-free composite passivation film are analyzed via scanning electron microscopy (SEM) and X-ray photoelectron spectroscopy (XPS). The effect of Mo on the corrosion resistance of the galvanized sheet is determined by means of an electrochemical method. In addition, the corrosion resistance of the galvanized sheet is verified via neutral salt spray tests.

2. EXPERIMENTAL

The experimental material: 600 mm × 100 mm × 0.5 mm cold-rolled hot-dip galvanized steel sheet (Panzhihua Iron & Steel Co., Ltd., Sichuan, China). Galvanized sheet passivation process: galvanized sheet → degreasing → washing → drying → coating → curing → cooling → finished product.

Preparation of the passivation solution: Take the silane coupling agent KH151 (CH_2=CHSi(OCH_2CH_3)$_3$, Shanghai Aladdin) and KH792 ($NH_2CH_2CH_2NHCH_2CH_2CH_2Si(OCH_3)_3$ in a molar ratio of 2:3 and add a certain amount of deionized water. 2) Add the remaining components in accordance with the dry weight percentage (shown in Table 1). A standing time of 24 h was required for the chromium-free composite passivation solution, prior to the coating process. Hexavalent chromium passivation solution, silane passivation solution, and galvanized bare plate are selected as a control group.

Table 1. Proportion of the main components comprising the chromium-free composite passivation solution

Component	Composite silane	Ammonium molybdate	Nano silica sol	Tannins
Proportion	3.88%	1.55%	3.53%	3.15%
Manufacturer	Shanghai Aladdin	Shanghai Aladdin	Shanghai Aladdin	Shanghai Aladdin

The surface morphology and elemental composition of a chromium-free composite passivation film and a silane passivation film were analyzed via field emission SEM (Quanta 650FEG, FEI Corporation, USA) and XPS (Kratos AXIS Ultra DLD, Shimadzu Corporation).

The corrosion resistance of a chromium-free composite passivation film, silane passivation film, hexavalent chromium passivation film, and galvanized bare plate were tested using a CHI760E electrochemical workstation (Shanghai Chenhua, China). An 803 saturated calomel electrode, a 99.99% platinum electrode, and a 0.5 mm × 10 mm × 10 mm galvanized plate specimen were used as the reference electrode, auxiliary electrode, and working electrode, respectively. Material was tested in an open system at room temperature with a 3.5% NaCl solution as the electrolyte. The open circuit potential-time curves were measured for three samples immersed in the electrolyte. Subsequently, the potentiodynamic polarization curves of the samples were measured at a rate of 0.5 mV/s from -1.5 to 1.5 VSCE with respect to the open circuit potential. The corrosion potential (E_{corr}) and corrosion current density (i_{corr}) were obtained using the Tafel extrapolation method; the polarization resistance (R_p) was obtained using the Stern-Geary equation [18]. The electrochemical AC impedance was measured in constant potential mode (frequency range: 100 kHz to 0.01 Hz) with a sinusoidal signal (amplitude: ±10 mV).

The 72-h neutral salt spray test was performed in a YWX / Q-020 Salt Spray Corrosion Test Chamber (Central Asia, China) on 0.5 mm × 75 mm × 150 mm samples. After the test was completed, the area percentage of white rust on the surface of the sample was evaluated.

3. RESULTS AND DISCUSSION

3.1. Surface Morphology and Phase Composition

Scanning electron micrographs of the silane passivation film and the chromium-free composite passivation film are shown in Fig. 1a and b, respectively. As shown in Fig. 1a, many micro-cracks surrounded by several other defects (such as zinc particles, zinc scars, and scratches) occur on the surface of the silane passivation film. These defects may damage the corrosive medium, leading to shedding of the film. The surface of the chromium-free composite passivation film is, in contrast, defect-free, indicating that this film can retard or eliminate the original defects of the galvanized sheet surface, thereby improving the surface quality (Fig. 1b). The elemental composition of the film is determined via energy dispersive spectroscopy (EDS; see Fig. 1c and d for the EDS spectrum of each sample). As Fig. 1c shows, the silane passivation film is composed mainly of elemental C, O, Zn accounting for fractions of 48.55%, 16.19%, and 27.40%, respectively, as well as P and Si. However,

the chromium-free film contains 1.13% Mo, occurring as a molybdate salt [13] (see Fig. 1d), and less Zn (occurring as partial Zn elements) than that occurring in the silane film.

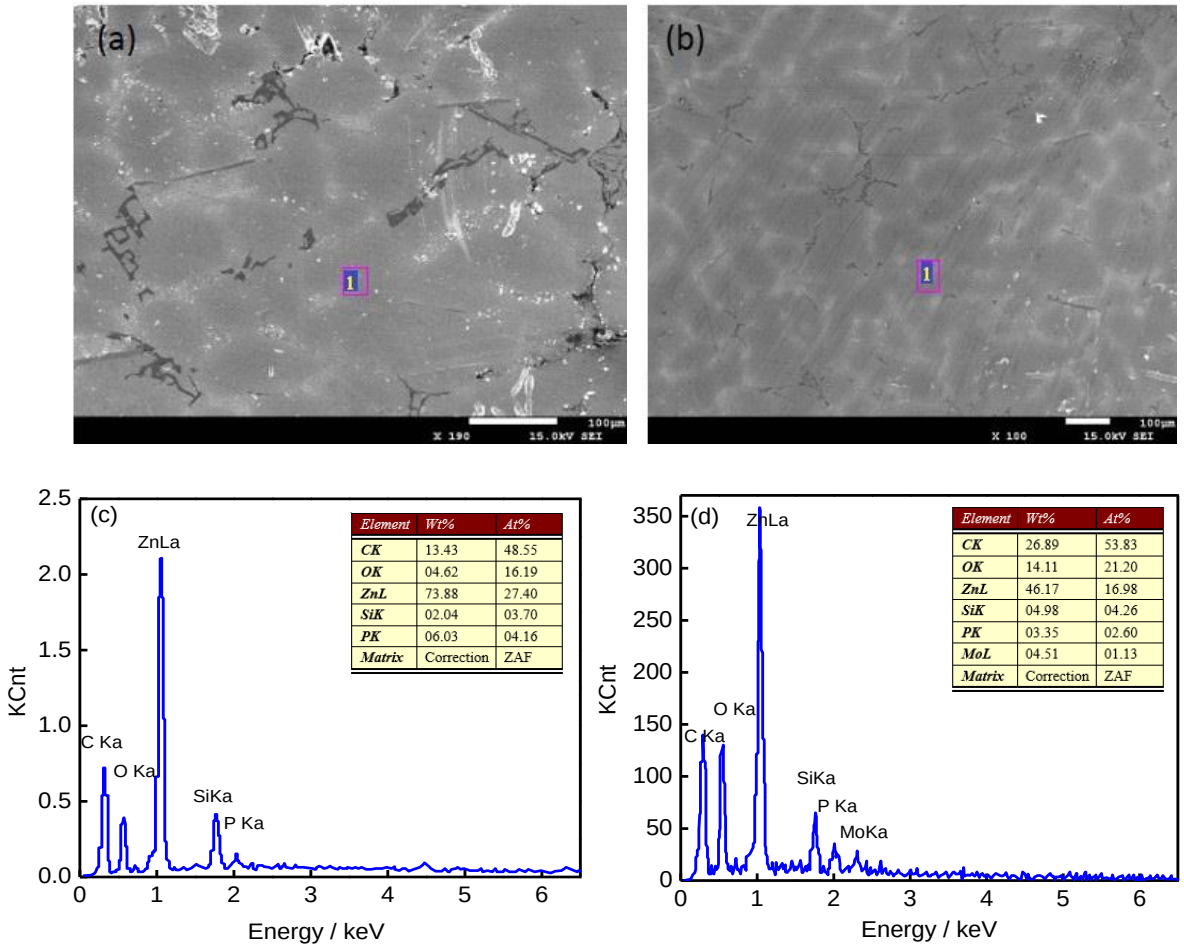

Figure 1. SEM image and EDS spectrum of silane passivation film and chromium-free composite passivation film (a), (c) silane passivation film and (b), (d) composite passivation film.

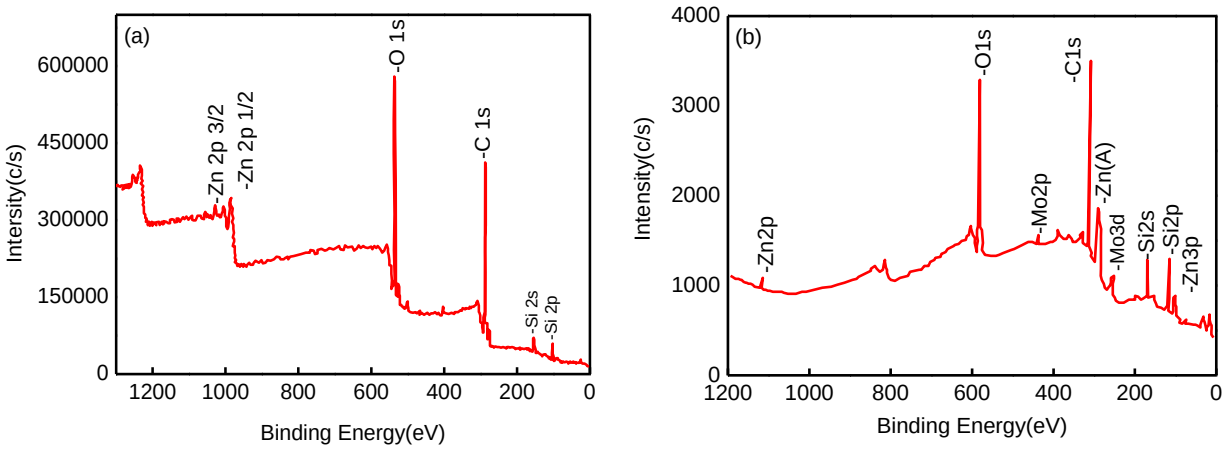

Figure 2. XPS photoelectron spectrum of the silane passivation film and the chromium-free composite passivation film (a) silane passivation film (b) chromium-free composite passivation film.

Figure 2 shows the full XPS spectrum of the silane passivation film and chromium-free composite passivation film. As shown in the figure, the silane film consists mainly of C, O, Si, and Zn, while the chromium-free film is composed mainly of C, Mn, O, Si, and Zn.

The valence of each element in the silane passivation film is determined by evaluating the narrow spectra (Fig. 3a–d) corresponding to the C, Si, O, and Zn in the film, respectively. Figure 3a reveals peaks at 285.66 eV, 284.80 eV, and 283.65 eV associated with the respective C-O, C-C [19–22], and C-Si bonds (due to the chemical shift resulting from the combination of C and Si elements) [23].

In Fig. 3b, the peak at 102.4 eV represents the Si-O-Si bond or the O-Si-O bond in the silane passivation film [24,25], and the peak at 102.8 eV represents Si-C bonds [26] or the Si-O-Zn bond. Similarly, the peaks at 531.2 eV, 532.7 eV, and 533.0 eV in Fig. 3c represent the Zn-O [27,28], Si-O [20], and C-O bonds, respectively. The peak at 1022.78 eV in Fig. 3d corresponds to Zn^{2+} and the peak at 1021.87 eV is associated with metallic Zn.

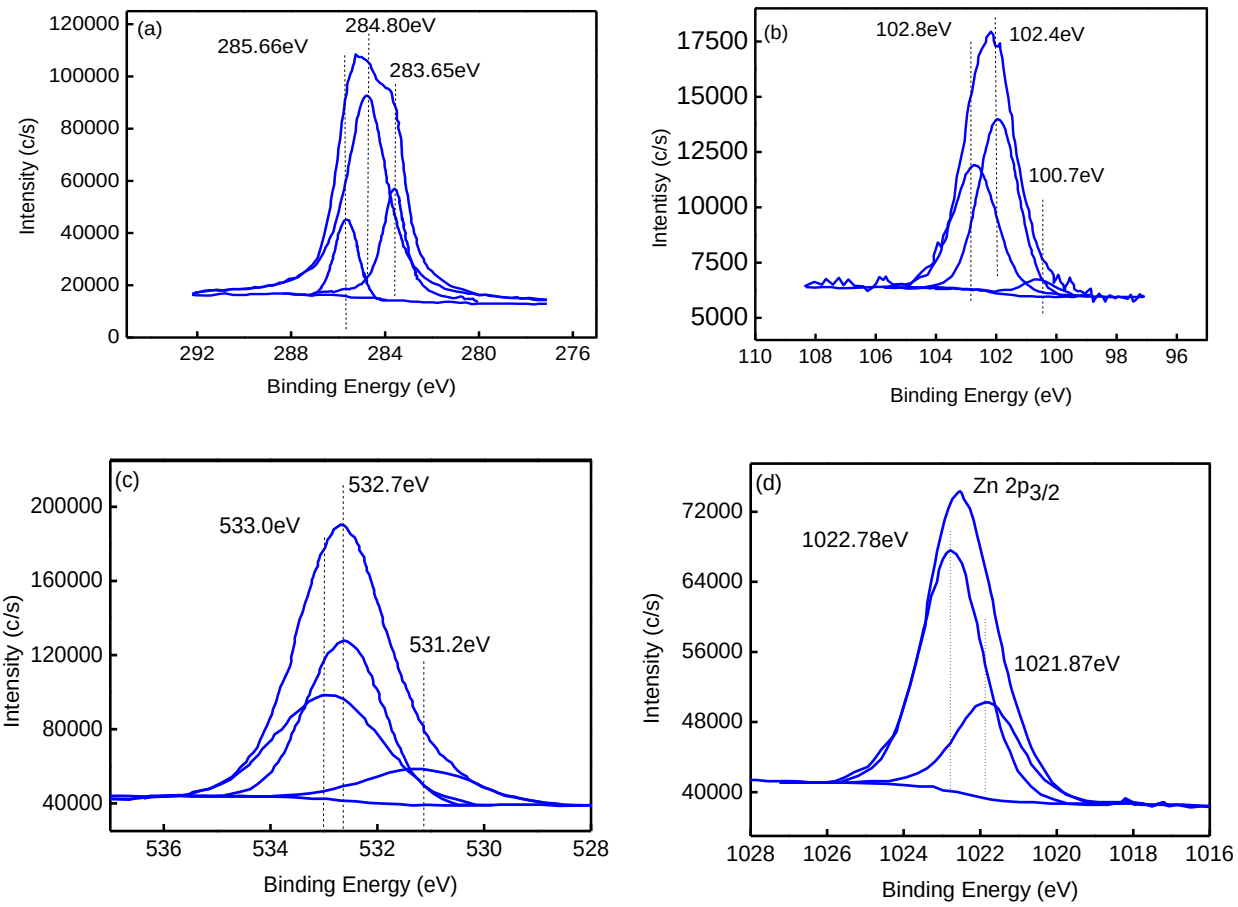

Figure 3. XPS narrow spectra of the silane passivation film (a) C element (b) O element (c) Si element (d) Zn element.

Figures 4a–d show the narrow spectra of elemental Mo, O, Si, and Zn contained in the chromium-free composite passivation film. In Fig. 4a, the peaks at 232.6 eV and 233.9 eV represent Mo^{6+} and Mo^{3+}, respectively. As the existential form of O in the film id O^{2-}/OH^-, Mo occurs in the form of MoO_4^{2-}, MoO_3, and $Mo(OH)_3$. In Fig. 4b, O on the surface of the passivation film occurs in the form of Mo_2O_3, Mo $(OH)_3$, MoO_4^{2-}/MoO_3, ZnO, and Zn $(OH)_2$. Figure 4c reveals that the Si-C bond at 102.8 is shifted by 0.4 eV with respect to the Si narrow spectra of the silane passivation film. This shift may have resulted from the fact that the addition of Mo facilitates Si-C bond formation. As Fig. 4d shows, most of the Zn occurs in the form of Zn^{2+}, indicating that the reaction of Mo with Zn generates $ZnMoO_4$.

In summary, in addition to the organic components introduced by silane, the inorganic components of the chromium-free composite passivation film include Mo_2O_3, $Mo(OH)_3$, MoO_3, Zn $(OH)_2$, $ZnMoO_4$, and $ZnMo_2O_4{\cdot}H_2O$. Previous studies [29,30] have shown that MoO_4^{2-} can block erosive anions, rendering the passivation layer cation-selective. In other words, Mo components have a significant effect on the passivation and can yield improved corrosion resistance of the chromium-free composite passivation film.

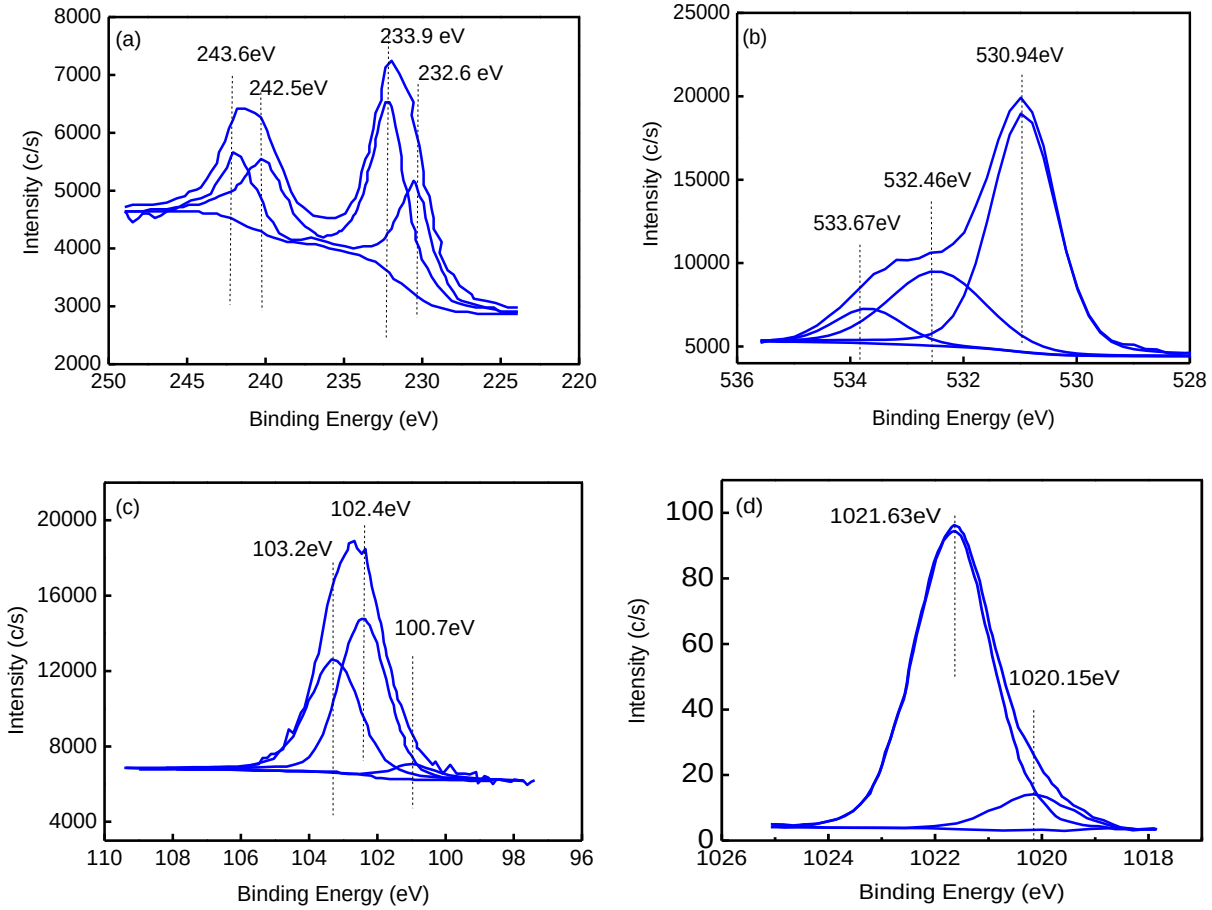

Figure 4. XPS narrow spectra of elemental (a) Mo, (b) O, (c) Si, and (d) Zn in the chromium-free composite passivation film.

3.2. Electrochemical Measurements

Figure 5 shows the potentiodynamic polarization curve of the hexavalent chromium passivation film, silane passivation film, chromium-free composite passivation film, and galvanized bare plate (dashed line). In the figure, the open corrosion potential of each passivation film is considerably lower than that of the bare galvanized steel sheet, indicating that the corrosion tendency of the films is weaker than that of the bare sheet.

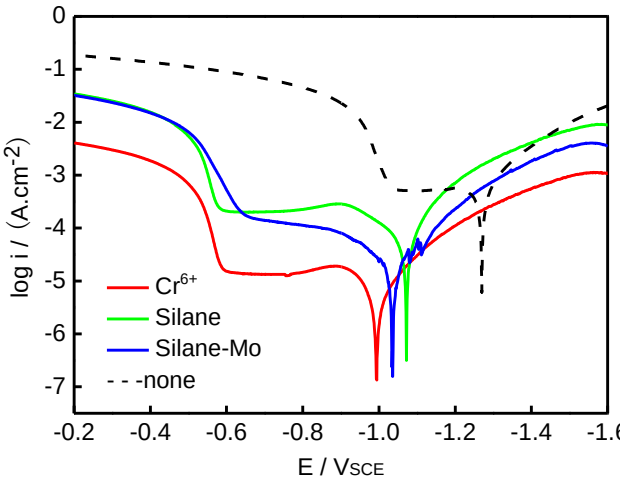

Figure 5. Potentiodynamic polarization curves of the silane passivation film, hexavalent chromium passivation film, chromium-free composite passivation film (dashed line denotes the galvanized bare plate).

The important parameters of the curve are shown in Table 2. As the table shows, the hexavalent chromium passivation film has the smallest current density and the largest polarization resistance. The corrosion current of the chromium-free composite passivation film is significantly smaller than that of the silane passivation film, and the polarization resistance has increased. Furthermore, the corrosion current density reflects and is directly proportional to the corrosion rate [31–33]. The reduction in the open corrosion potential density may have resulted from the formation of a passivation film on the surface, which retards the transfer of ions, thereby reducing the rate of corrosion. Therefore, the hexavalent chromium passivation film exhibits the best corrosion resistance, and the electrochemical parameter of the chromium-free passivation film approaches that of the hexavalent chromium passivation film.

Table 2. Free corrosion potential and current density of the hexavalent chromium passivation film and the chromium-free composite passivation film

Sample	E_{corr} (V_{SCE})	I_{corr} ($A \cdot cm^{-2}$)	R_p ($\Omega \cdot cm^{-2}$)
Cr^{6+}	-0.994	7.94×10^{-6}	5352
Silane	-1.072	3.03×10^{-5}	4597
Silane-Mo	-1.036	1.25×10^{-5}	5058

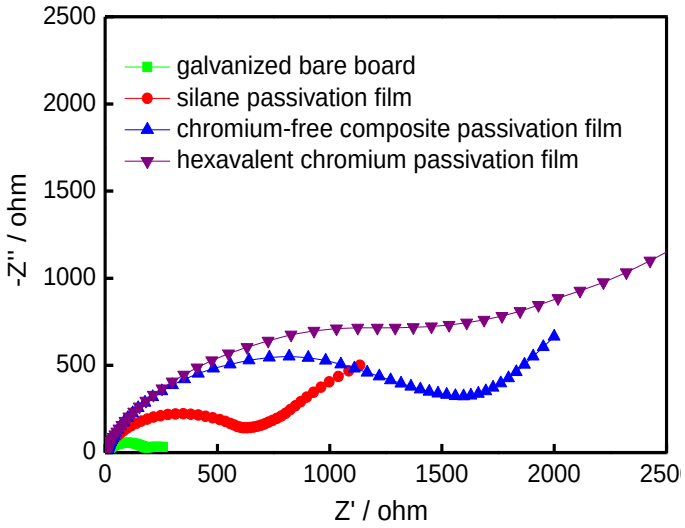

Figure 6. Electrochemical impedance spectroscopy of the silane passivation film, hexavalent chromium passivation film, chromium-free composite passivation film, and galvanized bare plate.

Figure 6 shows the electrochemical impedance spectroscopy results of different samples. The impedance values of the silane passivation film and chromium-free composite passivation film are significantly higher than that of the galvanized bare plate. In addition, the impedance value of the chrome-free composite passivation film is 1.6 times that of the silane passivation film, but is similar to the impedance value of the hexavalent chromium passivation film. The magnitude of the impedance value reflects the ease with which the electrolyte diffuses into the pores of the film. The amount of diffusion that occurs reflects the resistance of the passivation film to corrosion [34–36]. This means that the addition of molybdenum can yield significant improvement in the resistance of the film, inhibit the corrosion electrochemical reaction, and reduce the reaction rate, with the aim of mitigating galvanized sheet corrosion.

3.3. Neutral Salt Spray Experiment

The optimum amount of coating in actual production and the corrosion resistance of each passivation film are determined. For this determination, a chromium-free composite passivation film sample with different coating amounts is subjected to a 72-h neutral salt spray corrosion comparison test (see Fig. 7 for the corresponding results). Figure 7a and 7b show a sample of a silane passivation film and a sample of a hexavalent chromium passivation film, respectively, each with a coating amount of 780 mg/m^2. Figures 7c–f show the chromium-free composite passivation film samples with different coating amounts. A coating amount of 652 mg/m^2 for the chromium-free composite passivation film yields a corrosion area of >30% and a poor corrosion resistance. When the coating amount of this film reaches 780 mg/m^2, the corrosion resistance increases substantially, and the corrosion area is only ~2%–3%. However, the surface of the silane passivation film with the same coating amount undergoes severe corrosion. Combining these results with the SEM images indicates that corrosion begins at the

sites of the original defects (see Fig. 1a). This also indirectly confirms that the surface quality of the galvanized sheet plays an important role in determining the corrosion resistance of such sheets.

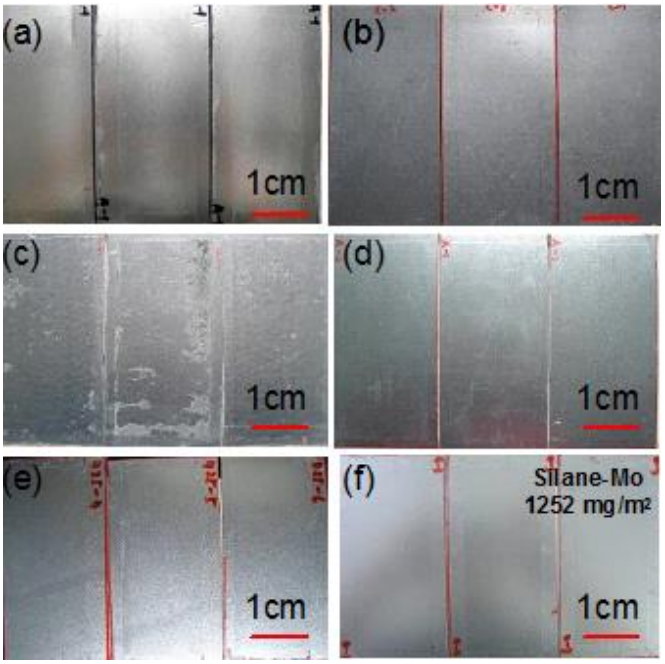

Figure 7. 72-h salt spray test results for silane passivation film, hexavalent chromium passivation film, and chromium-free composite passivation film. (a) silane passivation film-780 mg/m^2, (b) hexavalent chromium passivation film-780 mg/m^2, (c) chromium-free composite passivation film-652 mg/m^2**,** (d) chromium-free composite passivation film-780 mg/m^2, (e) chromium-free composite passivation film-892 mg/m^2, (f) chromium-free composite passivation film-1250 mg/m^2.

A comparison of Fig. 7c–f reveals that the corrosion resistance of the chromium-free composite passivation film on the surface of the galvanized sheet increases gradually with the weight of the film. Moreover, a surface corrosion area of zero is realized when the coating amount reaches 892 mg/m^2, and the corrosion resistance is equivalent to that of the hexavalent chromium passivation film. Excellent corrosion resistance is realized at a coating amount of 1252 mg/m^2.

4. CONCLUSION

1) The chromium-free composite passivation film has attributes of both a molybdate passivation film and an organosilane passivation film. Owing to these attributes, the film exhibits high resistance, corrosion electrochemical reaction is inhibited, reaction speed decreases, and corrosion resistance of the film increases significantly.

2) The chromium-free composite passivation film is uniform and compact. Mo inhibits the generation and development of micro-cracks, alleviates or eliminates the defects on the surface of the silane passivation film, and improves the surface quality.

3) The corrosion resistance of the chromium-free composite passivation film is significantly higher than that of the silane passivation film, and excellent corrosion resistance is realized at a coating amount of 1252 mg/m^2.

ACKNOWLEDGEMENTS
This project was supported by the National Natural Science Foundation of China (NO 51601081 and 51665022).

References

1. B.L. Lin, J.T. Lu, G. Kong, *Corros. Sci.*, 50 (2008) 962.
2. X.H. Yu, Z.L. Zhan, *Nanoscale Res. Lett.*, 9 (2015) 516.
3. H.C. Yu, X.Y. Huang, F.H. Lei, X.C. Tan, Y.Y. Han, *Surf. Coat. Tech.*, 218 (2013) 137.
4. X.H. Yu, J. Rong, Z.L. Zhan, Z. Liu, J.X. Liu, *Mater. Design.*, 83 (2015) 159.
5. C. Liu, J. Rong, Y.N. Zhang, X.H. Yu, J.X. Liu, Z.L. Zhan, *Int. J. Electrochem. Sci.*, 12 (2017) 9914.
6. D.L. Liu, Z.G. Yang, Z.Q. Wang, C. Zhang, *Surf. Coat. Tech.*, 205 (2010) 2328.
7. J. Rong, M. Kun, X.H. Yu, Y.N. Yang, *Int. J. Electrochem. Sci.*, 12 (2017) 11987.
8. X. Wang, Y.N. Yang, C. Liu, Z.T. Yuan, X.H. Yu, Y. Zhong, Z.L. Zhan, *Int. J. Electrochem. Sci.*, 12 (2017) 12009.
9. X.H. Yu, Z.L. Zhan, J. Rong, Z. Liu, L. Li, J.X. Liu, *Chem. Phys. Lett.*, 600 (2014) 43.
10. Q. Cheng, C. Liu, K. Meng, X.H. Yu, Y.N. Zhang, J.X. Liu, X. Jin, L.Y. Jin, *Int. J. Electrochem. Sci.*, 13 (2018) 265.
11. V.R. Capelossi, I.V. Aoki, *Prog. Org. Coat.*, 76 (2013) 812.
12. D.Q. Zhu, W.J. Ooij, *Prog. Org. Coat.*, 48 (2004) 42.
13. H. Yang, X. Kong, W. Lu, Y. Liu, J. Guo, S. Liu, *Prog. Org. Coat.*, 67 (2010) 375.
14. P. Wang, D. Zhang, R. Qiu, B. Hou, *Corros. Sci.*, 53 (2011) 2080.
15. R. Qiu, D. Zhang, P. Wang, *Corros. Sci.*, 66 (2013) 350.
16. E. Faure, E. Halusiak, F. Farina, N. Giamblanco, C. Motte, M. Poelman, C. Archambeau, C.V.D. Weerdt, J. Martial, C. Jérôme, A.S. Duwez, C. Detrembleur, *Langmuir*, 28 (2012) 2971.
17. V. Saarimaa, A. Markkula, J. Juhanoja, B.J. Skrifvars, *J. Coat. Sci. Tech.*, 1 (2014) 88.
18. Z.Q. Tan, C.M. Hansson, *Corros. Sci.*, 50 (2008) 2512.
19. L. Wang, C.S. Liu, H.Y. Yu, C.Q. An, *J. Iron Steel Res. Int.*, 19 (2012) 46.
20. G. Kong, J. Lu, H. Wu, *J. Rare Earth.*, 27 (2009) 164.
21. C. Zhou, X. Lu, Z. Xin, J. Liu, *Corros. Sci.*, 70 (2013) 145.
22. C. Zhou, X. Lu, Z. Xin, J. Liu, Y. Zhang, *Corros. Sci.*, 80 (2014) 269.
23. L.K. Wu, J.T. Zhang, J.M. Hu, J.Q. Zhang, *Corros. Sci.*, 56 (2012) 58.
24. A.J. Jose, M. Alagar, F. Chacko, *Appl. Clay Sci.*, 71 (2013) 64.
25. Z.A. Hamid, A.A. Aal, H.B. Hassan, A. Shaaban, *Appl. Surf. Sci.*, 256 (2010) 4166.
26. N. Michailidis, F. Stergioudi, G. Maliaris, A. Tsouknidas, *Surf. Coat. Tech.*, 259 (2014) 456.
27. R.B. Figueira, C.J.R. Silva, E.V. Pereira, *J. Coat. Technol. Res.*, 12 (2015) 1.
28. S. Liu, H. Sun, L. Sun, H. Fan. *Corros. Sci.*, 65 (2012) 520.
29. C.Y. Tsai, J.S. Liu, P.L. Chen, C.S. Lin. *Corros. Sci.*, 52 (2010) 3385.
30. E. Sarmiento, J.G. González-Rodriguez, J. Uruchurtu, O. Sarmiento, M. Menchaca, *Int. J. Electrochem. Sci*., 4 (2009) 144.
31. M. Fouladi, A. Amadeh, *Electrochim. Acta*, 106 (2013) 1.
32. M. Carbucicchio, R. Ciprian, F. Ospitali, G. Palombarini, *Corros. Sci.*, 50 (2008) 2605.
33. H.Y. Su, C.S. Lin, *Corros. Sci.*, 83 (2014) 137.

34. A.M.P. Simões, R.O. Carbonari, A.R. Di Sarli, B. Del Amo, R. Romagnoli, *Corros. Sci.*, 53 (2011) 464.
35. X. Zhang, G.Y. Xiao, C.C. Jiang, B. Liu, N.B. Li, R.F. Zhu, Y.P. Lu, *Corros. Sci.*, 94 (2015) 428.
36. L. Pezzato, K. Brunelli, E. Napolitani, M. Magrini, M. Dabalà, *Appl. Surf. Sci.*, 357 (2015) 1031.